STUDIA UBB CHEMIA, LXIII, 4, 2018 (p. 15-29)
(RECOMMENDED CITATION)
DOI:10.24193/subbchem.2018.4.02

Dedicated to the Memory of Assoc. Prof. RNDr. Daniel Nižňanský (1963-2018)

FRACTAL SURFACE MAGHEMITE NANOPARTICLES PREPARED BY CO-PRECIPITATION: THE INFLUENCE OF IRON CONCENTRATION AND BASE NATURE

ROXANA NICOLA (CRIŞAN)[a], OTILIA COSTIŞOR[a], CĂTĂLIN IANĂŞI[a], RADU LAZĂU[b], LIVIU SĂCĂRESCU[c], DANIEL NIŽŇANSKÝ[d], AUREL ERCUŢA[e], ANA-MARIA PUTZ[a], CECILIA SAVII[a,*]

ABSTRACT. Two series of magnetic nanopowders were synthesized at room temperature starting from a mixture of iron II and III precursors, $FeSO_4$ and $FeCl_3$, respectively. Precipitation agents, as KOH and NaOH were used. While the concentration of the added ferrous and ferric solutions ranged between 0.1 M and 0.0125 M, the hydroxide solution concentration was maintained constant (1 M). TEM images of the samples showed that the particles shape changes from quasi spherical to spherical. For both series the crystallite size decreases with iron concentration, from 9 to 2 nm for KOH series and from 10 to 3 nm for NaOH series. Moessbauer Spectroscopy was signaling only Fe^{3+} in the final spinel product. BET measurements revealed the material mesoporosity and fractal structure of maghemite nanoparticles that explain the unusual high surface area, ~240 m^2/g. All the samples actually exhibit superparamagnetic behavior at room temperature with saturation magnetization up to 73 emu/g value closed to those of bulk maghemite.

Keywords: *iron oxide nanoparticles, co-precipitation, fractal surface, Moessbauer Spectroscopy.*

[a] *Institute of Chemistry Timişoara of Romanian Academy, Laboratory of Inorganic Chemistry, Mihai Viteazul Bd., No. 24, 300223, Timişoara, România.*
[b] *"Politechnica" University of Timişoara, Faculty of Industrial Chemistry and Environmental Engineering, Vasile Pârvan Bd., No. 6, 300223, Timişoara, România.*
[c] *Institute of Macromolecular Chemistry "Petru Poni", Grigore Ghica Voda Alley, No. 41A, 700487, Iaşi, România.*
[d] *Charles University in Prague, Faculty of Science, Albertov 6, 128 43, Praque, Czech Republic.*
[e] *West University of Timisoara, Faculty of Physics, Vasile Pârvan Bd., No. 4, 300223, Timişoara, România.*
[*] *Corresponding author: ceciliasavii@yahoo.com*

INTRODUCTION

The synthesis of superparamagnetic nanoparticles has been intensively developed because they are used in many applications, such as: magnetic storage media (e.g. magnetic carbon nanotubes composites [1], catalysts, magnetic fluids, sensors [2], as anode for lithium-ion (LIBs) [3] and sodium-ion (SIBs) [4] batteries, MRI contrast agent [5], tissue repair [6], detoxification of biological fluids, hyperthermia [7], cell and protein separation [8] and drug delivery [9][10][11].

Several synthesis methods like co-precipitation [12], microemulsion [13], thermal decomposition [14], solvothermal [15], sonochemical [16] are commonly used to produce magnetic nanoparticles. Chemical co-precipitation appears to be the most promising method, due to its simplicity, productivity and low cost [17]. In general, precipitation of magnetite requires a Fe^{3+}/Fe^{2+}ratio of 2:1, and pH values between 8 and 14 [18].

Numerous studies demonstrate that several factors like pH [19], temperature [20], ionic strength [21], nature of salts [22], Fe^{2+}/Fe^{3+} ratio [23], iron concentration [24], type of the precipitant agent [25] etc. affect the size and size distribution of the iron oxide nanoparticles.

Iron ion concentration is an important parameter because it has influence upon size and magnetic properties of nanoparticles. According to LaMer theory [26], at supersaturation, a critical concentration is defined as the nuclei start to grow by atomic species diffusion from solution towards the particles surfaces.

Fe oxide nanoparticles having a mesoporous structure are of interest for biomedical applications, due to the fact that the presence of mesopores facilitates high active agents loading [27]. Also, nanoparticles with high surface area can be used in catalysis [28], or as adsorbents, e.g. for heavy metal ions removal from waste water [29].

The present paper proposes a simple and economic synthesis route to obtain mesoporous maghemite nanoparticles with high surface area, exhibiting superparamagnetic behavior at room temperature.

Co-precipitation method presents advantages and disadvantages. Compared to other chemical methods, it is simple, low cost and environmentally friendly (not using organic solvents and directing agents), mild temperature conditions [30]. It is well known, the main requirements regarding magnetic nanoparticles properties with potential use in biomedical applications, such as: to be hydrophilic, nontoxic, biocompatible, near spherical, and mesoporous etc. [9][31]. Among mentioned essentials is that to be obtained in soft conditions (low temperature, aqueous media etc.).

As main disadvantage that can be mentioned was that the co-precipitation method does not always assures a perfect spherical shape of the particles and narrow particle size distribution. We agree other researchers opinion that sometimes it is worthless to expend time, money and effort designing definite particle properties (by using sophisticated preparing protocols), since co-precipitation was able to generate suitable particles for target applications [32].

The subject, the present work is dealing with, apparently was a common task, because in time, a great number of scientist published about iron oxide based magnetic nanomaterials properties (crystalline structure, magnetic properties etc.) in relationship with preparation variables (concentration of iron oxide precursor, nature of base as precipitating agent). To our best knowledge there are relatively few references where the morpho-textural properties of magnetic materials were discussed in relationship with both synthesis parameters and desired functionalities. In literature, the morpho-textural parameters are rarely reflected at the same level as crystallinity and magnetic properties. In the paper, besides crystalline and magnetic ordering, we mainly discussed morpho-textural properties related to synthesis conditions. Concerning preparation method, in order to avoid the pH local altering [33], we have chosen the reversed co-precipitation route, also less reported in iron oxide synthesis references.

RESULTS AND DISCUSSIONS

Transmission electron microscopy

In **Figure 1** the TEM images of samples $K_{0.1}$, $K_{0.025}$, $K_{0.0125}$, $N_{0.1}$, $N_{0.025}$ and $N_{0.0125}$ samples are shown. The TEM image of $K_{0.1}$ sample shows particles of spherical shape and narrow size distribution (6 -15 nm), while the particles shape in $K_{0.025}$ and $K_{0.0125}$ samples changes to quasi spherical, and the size distribution is centered on 5 nm and 3 nm respectively. The TEM images of the NaOH-base samples $N_{0.1}$, $N_{0.025}$ and $N_{0.0125}$ show the same particle size and distribution evolution pattern. It was observed that for both series, the particles size of maghemite decreases as the iron precursor concentration decreases.

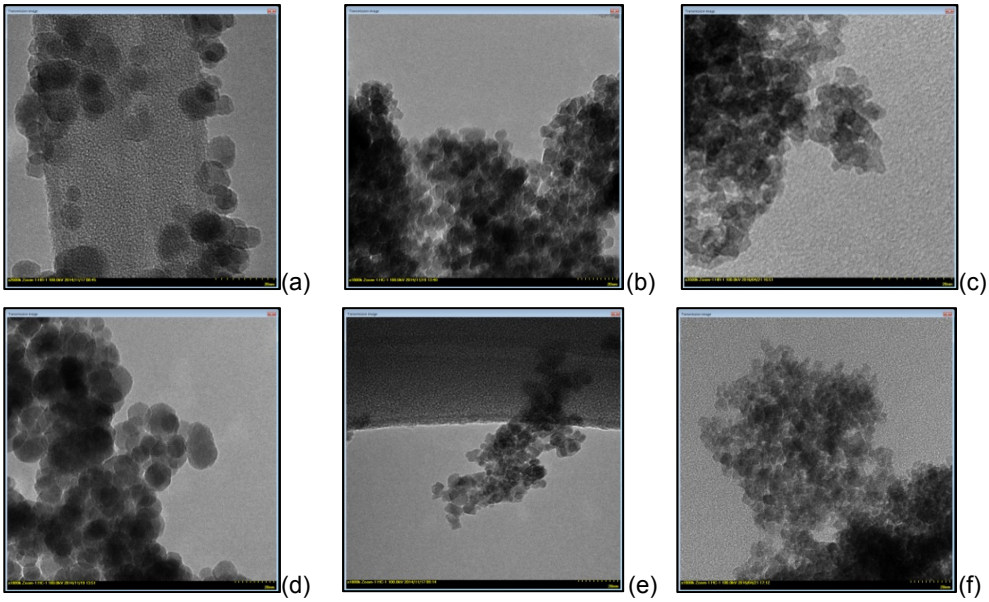

Figure 1. TEM images of samples: (a) $K_{0.1}$, (b) $K_{0.025}$, (c)$K_{0.0125}$, (d) $N_{0.1}$, (e) $N_{0.025}$ and (f) $N_{0.0125}$ (scale bar: 20 nm)

X-Ray powder diffraction analysis

The XRD spectra of the samples were recorded; as visible in **Figure 2**, all the spectra exhibit the characteristic lines of the cubic spinel structure (PDF file no. 00-039-1346).

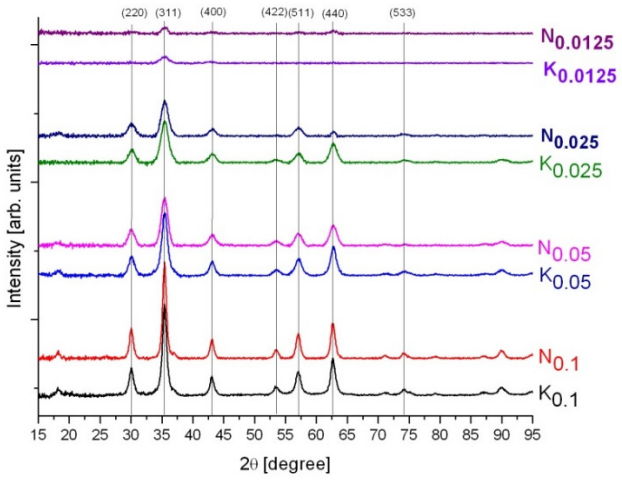

Figure 2. XRD spectra of synthesized iron oxide nanoparticles

It can be observed that the decrease of Fe concentration leads to diffraction peaks broadening, which indicates poor crystallization and/or small particle size. Also, the samples $K_{0.1}$-$K_{0.0125}$ samples exhibit higher degree of crystallinity (the Bragg peaks are narrower) compared $N_{0.1}$-$N_{0.0125}$ samples. The crystallite size and lattice parameter data of the two sample series are summarized in **Table 1**.

Table 1. Crystallite size and lattice parameter of the samples

KOH series	Average size of crystallite estimated by XRD [nm]*	Lattice parameter [nm]	NaOH series	Average size of crystallite estimated by XRD [nm]*	Lattice parameter [nm]
$K_{0.1}$	8.8	0.8393	$N_{0.1}$	9.8	0.8393
$K_{0.05}$	6.5	0.8389	$N_{0.05}$	5.7	0.8377
$K_{0.025}$	4.6	0.8384	$N_{0.025}$	4.6	0.8387
$K_{0.0125}$	2.0	0.8404	$N_{0.0125}$	2.7	0.8389

* calculated by using WPPF method

As the Fe concentration decreases from 0.1 M to 0.0125 M, the average crystallite size decreases from 8.8 to 2.0 nm and from 9.8 to 2.7 nm (**Table 1**), for samples synthesized with KOH and with NaOH, respectively.

The XRD data (crystallite size calculated with WPPF method) are consistent with TEM results. It can be observed that the particle size as visible in the TEM images is consistent with the crystallite size resulting from XRD data. It follows that the crystallites are slightly aggregated and a particle is composed by one or two agglomerated crystallites.

Moessbauer Spectroscopy

Both, magnetite and maghemite (except for vacancy ordered) exhibit similar XRD patterns, which makes difficult their identification. To facilitate the differentiation of the iron ionic species, Moessbauer Spectroscopy measurements were carried out for samples $K_{0.1}$, $K_{0.0125}$, $N_{0.1}$ and $N_{0.0125}$. In **Figure 3** room temperature Moessbauer spectra (MS) are shown.

It is common knowledge that MS showing sextet(s) belong to magnetically ordered phases of iron oxides [34]. Generally, in order to show sextet(s), the iron oxide particle dimension must be greater than its critical particle size having blocking temperature around room temperature. In the case of magnetite or maghemite, the critical particle size approximately corresponds to 10 nm.

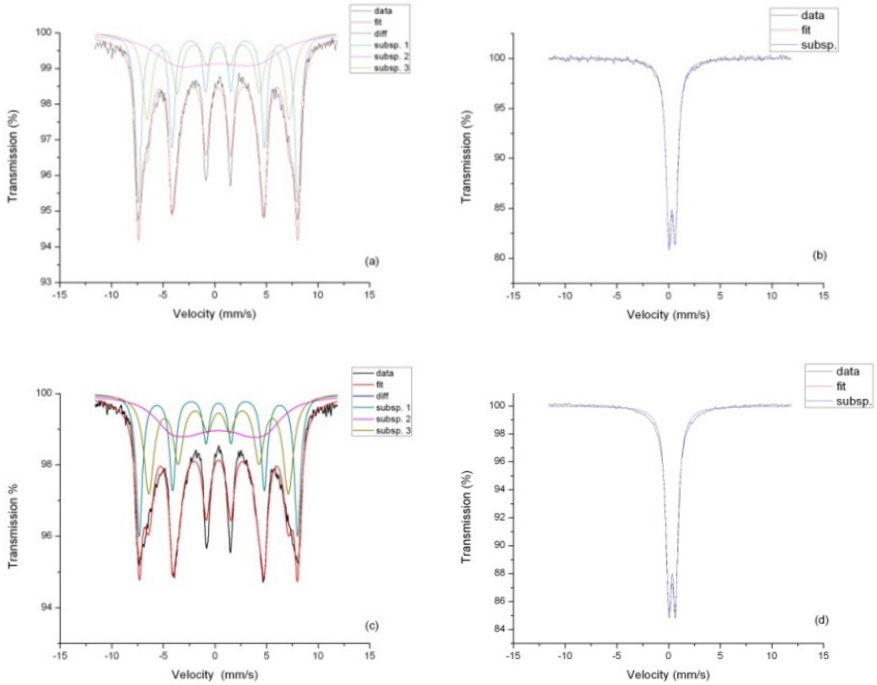

Figure 3. Room temperature MS of (a) $K_{0.1}$, (b) $K_{0.0125}$, (c) $N_{0.1}$ and (d) $N_{0.0125}$

So, we can conclude that the samples prepared using 0.1 M iron precursor solutions contain larger nanoparticles (> 10 nm) whereas using 0.0125 M solutions for the preparation leads to smaller particles (< 10 nm) as it was confirmed by the determination of crystallite size from XRD and particle size resulted from TEM.

Table 2. Parameters of $K_{0.1}$, $K_{0.0125}$, $N_{0.1}$ and $N_{0.0125}$ samples obtained from Moessbauer measurements

Sample	Isomer shift (IS) δ [mm/s]	Quadrupole splitting ΔE_Q [mm/s]	Hyperfine field B_{Hf}	Relative area (%)	Attribution
$K_{0.1}$	(1)0.33 (2)0.35 (3)0.34	(1)-0.0035 (2)-0.0380 (3)-0.0013	(1)47.70 (2)28.41 (3)42.00	(1)32 (2)33 (3)35	maghemite maghemite maghemite
$K_{0.0125}$	(1)0.33	(1)0.6394		(1)100	maghemite
$N_{0.1}$	(1)0.33 (2)0.16 (3)0.35	(1)-0.0061 (2)0.1326 (3)-0.0252	(1)47.96 (2)27.08 (3)42.77	(1)39 (2)30 (3)31	maghemite maghemite maghemite
$N_{0.0125}$	(1)0.33	(1)0.6642		(1)100	maghemite

MS give us the information about the oxidation state of iron through the value of isomer shift. In the above MS, the isomer shift (IS) values are situated in the range of 0.2– 0.4 mm/s which are characteristic values for Fe^{3+} (see **Table 2**). Reference values of IS for magnetite are around 0.26 mm/s in the case of Fe^{3+} in tetrahedral positions and 0.66 mm/s for Fe^{2+} and Fe^{3+} in octahedral sublattice. It means, that non-protected magnetite nanoparticles were oxidized by O_2 in air either in the early stage just after preparation or later during the samples storage in non-inert atmosphere.

Magnetite (Fe_3O_4) and maghemite (γ-Fe_2O_3) are common magnetic iron oxides that have spinel structure. Normal spinel structure is represented by$(A)_A[B_2]_BO_4$, where A stands for tetrahedral sites occupied by bivalent ions, and B stands for octahedral sites occupied by trivalent ions. In the case of inverse spinels, the tetrahedral positions are occupied by trivalent atoms. The unit cell formula of magnetite (inverse spinel) can be written as: $(Fe^{3+})_A[Fe^{2.5+}]_BO_4$, where the valence of iron in the octahedral sites is $Fe^{2.5+}$, due to the fast electron hopping above the Verwey transition, which take place around 121 K. Magnetite is sensitive to air expose, oxidizes, leading to nonstoichiometric magnetite, described by the formula: $(Fe^{3+})_A[Fe^{2+}_{1-3x}Fe^{3+}_{1+2x}\Upsilon_x]_BO_4$, where Υ denotes vacancy and are assumed to be located in octahedral sites in spinel structure and x ranges (0;1/3), where “0” stands for pure magnetite and “1/3” stands for pure maghemite. The fast electron hopping, which is known to be a pair-localized phenomenon in magnetite, results in $Fe^{2.5+}$ equal amounts of octahedral Fe^{2+} and Fe^{3+}: $(Fe^{3+})_A[Fe^{2.5+}_{2(1-3x)}Fe^{3+}_{5x}\Upsilon_x]_BO_4$. Maghemite is fully oxidized magnetite, where x=0.33 and general formula is $(Fe^{3+})_A[Fe^{3+}_{5/3}\Upsilon_{1/3}]_BO_4$ [35][36].

Textural analysis

Specific surface area, total pore volume, mean pore size, particle diameter and surface fractal dimension (D_s) are presented in **Table 3** and **Table 4** derived from N_2 adsorption-desorption isotherms presented in **Figure 4**. Assuming all the particles of spherical shape and equal size, the particle diameter was calculated using data from adsorption-desorption isotherm, using the following equation [27]:

$$D = \frac{6}{S_{sp}\rho_a} \quad (1)$$

where S_{sp} is the specific surface area and ρ_a is the density; for all maghemite samples a value of 4.9 g/cm^3 was considered.

BET derived particle size evaluations (Eq. (1)) (see **Tables 3** and **4**) are consistent with TEM results and XRD data.

Table 3. Results of textural data from adsorption-desorption isotherm for KOH series

Sample	Specific surface area [m^2/g]	Total pore volume [cc/g]	Mean pore size [nm]	Particle diameter approximated using specific surface area	D_s
$K_{0.1}$	91.01	0.2302	6.62	13.5	2.50
$K_{0.05}$	120.05	0.1871	4.92	10.2	2.61
$K_{0.025}$	152.21	0.1651	3.82	8.0	2.71
$K_{0.0125}$	239.65	0.2050	3.43	5.1	2.79

Table 4. Results of textural data from adsorption-desorption isotherm for NaOH series

Sample	Specific surface area [m^2/g]	Total pore volume [cc/g]	Mean pore size [nm]	Particle diameter approximated using specific surface area	D_s
$N_{0.1}$	80.50	0.2350	6.58	15.2	2.47
$N_{0.05}$	148.75	0.4421	6.61	8.2	2.48
$N_{0.025}$	160.54	0.3263	6.60	7.6	2.55
$N_{0.0125}$	219.52	0.4070	6.49	5.6	2.56

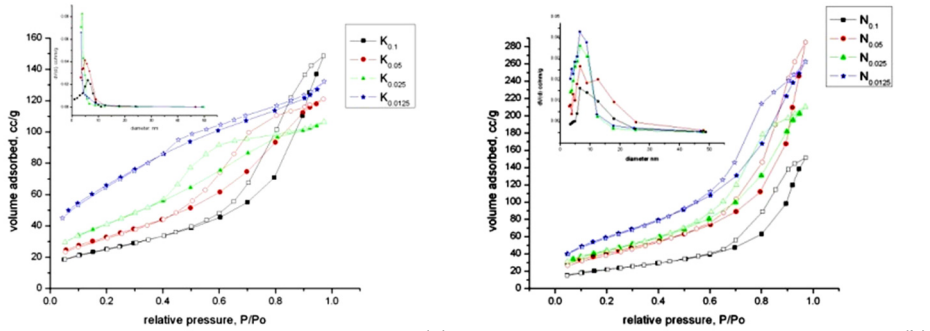

Figure 4. N_2 adsorption-desorption isotherms of (a) $K_{0.1}$, $K_{0.05}$, $K_{0.025}$ and $K_{0.0125}$, and (b) $N_{0.1}$, $N_{0.05}$, $N_{0.025}$ and $N_{0.0125}$. Inset: Pore size distribution curves of the samples

With the particle size decrease, in the case of sample series $K_{0.1}$-$K_{0.0125}$, the mean pore size also decrease, **Table 3**, and the specific surface area is increasing as was expected. In the case of the samples precipitated by NaOH, **Table 4**, this tendency is not so straightforward. The specific surface area regularly increases but the mean size of pores remains almost constant. So, we can see that the used basic reagents have different impact on the morphology of the aggregates.

One can see that the specific surface area is increasing with the decrease of iron precursor concentration, **Tables 3** and **4** leading to the particle size diminution. This tendency was in agreement with XRD and TEM results, the Sherrer derived crystallite size and particle size deduced from TEM also showed a decreasing trend with iron concentration.

The surface fractal dimension D_s was deduced by using Quantacrome Nova 1200e apparatus output and software, applying Frenkel-Halsey-Hill (FHH) equation [37]. All prepared samples contained iron oxide nanoparticles with apparently rough surface, having fractal structure, which can be characterized by surface fractal dimension, D_s. There was a clear increasing trend of D_s in both maghemite prepared series, specifically $2.50 \leq D_s \geq 2.79$ for KOH series and $2.47 \leq D_s \geq 2.56$, for NaOH series. A perfectly smooth surface has the value of surface fractal dimension $D_s=2$, while a highly rough surface has $D_s=3$ [38]. The obtained iron oxide particles present unusual high surface area that can be explained by its rugosity, well described by the surface fractal dimension, D_s, its evolution with iron precursor concentration was in perfect accord with the corresponding surface area trend.

The adsorption-desorption isotherms of all investigated samples correspond to a type IV-isotherm according to the Brunauer, Deming, Deming and Teller (BDDT) method, showing hysteresis [39]. The type IV isotherm was attributed to mono and multilayer adsorption and hysteresis loop is associated with capillary condensation in mesopores. These hysteresis loops are associated with mesoporous materials (containing pores between 2-50 nm diameter) [IUPAC]. In **Figure 4** are presented N_2 adsorption-desorption isotherms of the samples. Pore size distributions (calculated from desorption branch) of the samples are shown in **Figure 4** (inset). According to IUPAC classification, isotherms of $K_{0.1}$ and $N_{0.05}$ follows a H3 hysteresis loop type, as illustrated in **Figure 4**, which is observed with non-rigid aggregates of plate-like particles, giving rise to slit shape pores. For $K_{0.05}$ and $K_{0.025}$ typical hysteresis loop is type H2, and this hysteresis type is typical for materials with no uniform pore shapes and/or size. The H2 type adsorption hysteresis is associated with highly interconnected pores with ink-bottle shapes [40][41]. H1-type hysteresis loops of $N_{0.1}$, $N_{0.025}$ and $N_{0.0125}$ samples are associated with porous materials known to consisting of approximately uniform spheres aggregates in fairly regular array and hence to have narrow distribution of pore size. On the other hand $K_{0.0125}$ sample isotherm exhibits H4 hysteresis type, which appears to be associated with narrow slit-like pores [42].

A pore size distribution ranging in the mesopore domain is the main characteristic of all samples. It can be noted that samples from KOH series have a narrower pore size distribution than the samples from NaOH series.

In **Figure 4** inset, it can be seen that all the samples are characterized by mesoporous structures mainly consisting in slit-like pores. The slit-like pore geometry was recommended to be characterized using the concept of "pore width", which value, in our case, was ranging between 2 and 15 nm [43].

Magnetic properties characterization

Table 5. Magnetic parameters

Sample	Ms [emu/g]	Hc [kOe]	Mr [emu/g]	Squareness ratio Mr/Ms	Sample	Ms [emu/g]	Hc [kOe]	Mr [emu/g]	Squareness ratio Mr/Ms
$K_{0.1}$	73.3	0.053	6.1	0.08	$N_{0.1}$	66.3	0.04	6.35	0.1
$K_{0.05}$	64.5	0.024	1.8	0.03	$N_{0.05}$	60.7	0.005	0.27	0.004
$K_{0.025}$	43.9	0.014	0.6	0.01	$N_{0.025}$	44.7	0.014	0.42	0.009
$K_{0.0125}$	30.1	0.03	0.17	0.005	$N_{0.0125}$	29.9	0.015	0.16	0.005

Room temperature magnetic measurements of all synthesized iron oxide samples indicate that the nanoparticles exhibit superparamagnetic behavior; the results are summarized in **Table 5**, **Figure 5**. According to literature, the squareness ratio of hysteresis loop, expressed by Mr/Ms ratio, less than 0.1 could categorize the magnetic material as superparamagnetic metal oxide crystals [44].

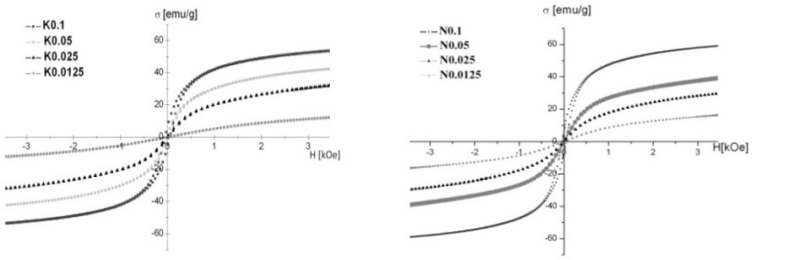

(a) (b)

Figure 5. Magnetization curves (a) KOH series and (b) NaOH series

Saturation magnetization M_s increases, as it was expected, with the iron concentration and crystallite size respectively (see **Table 5**). Specifically, in the case of KOH based samples, M_{smax} value of 73.3 emu/g was found for the highest iron concentration sample, $K_{0.1,}$ of 0.1 M in the given conditions. When NaOH was used, also the corresponding $N_{0.1}$ sample showed the max M_s value of 66.3 emu/g (see **Table 5**). It can be noted that KOH series exhibited higher values of M_s comparing NaOH one. A possible explanation might be

because the KOH series maghemite particles present significantly better crystallinity. This assumption is supported by the XRD patterns features presented in **Figure 2**.

On account of the surface disorder and modified cationic distribution, smaller particles exhibit smaller values of M_s, due to the pronounced surface effects in nanoparticles [45][46]. The surface region of the nanoparticles is assumed to be composed of some canted or disordered spins that prevents the spins from aligning along the field direction, thus resulting a decrease of M_s [46][47]. The spin disorder layer increases with the decrease in crystallite size [48]. It cannot be neglected the contribution of the effect of dipolar interaction between nanoparticles [27][49] and or of the magnetic phase poor crystallinity [50] to the reduction of the material global magnetic moment.

CONCLUSIONS

Spinelic magnetic nanoparticles systems were obtained by reverse co-precipitation (Fe^{2+}/ Fe^{3+}) in a large window of pH and precursors concentrations, by using KOH or NaOH.

As general conclusions, it can be noted that: pure superparamagnetic maghemite was obtained; the particles size of maghemite samples decreases with iron precursor concentration; the average crystallite size was situated up to 10 nm, slightly depending on the base nature too; the maghemite nanoparticle shape was improved from quasi spherical to spherical as Fe concentration increases.

In particular, for exclusive crystalline materials, unusual high surface area was obtained, of ~239 m^2/g and ~219 m^2/g, for $K_{0.0125}$ and $N_{0.0125}$ samples, respectively. N_2 adsorption – desorption isotherms data (FHH method) allowed to evaluate the apparent fractal character of obtained materials and to calculate the surface fractal dimension, Ds. Such way, by considering the fractal character of particle surface was possible to evaluate surface rugosity trend, that was consistent to corresponding surface areas and to be related to precursors concentrations. The lower precursor concentration leads to the higher rugosity and the higher surface area.

In spite of relatively low particle size, the prepared samples showed high saturation magnetization, M_s (e.g. ~73 emu/g), closed to the M_s value (~90 emu/g) of the bulk maghemite.

High surface areas and generous total pore volume of synthesized samples together with crystalline and magnetic properties, recommend them as potential candidates for catalysis domain and biomedical applications, as drug carriers.

EXPERIMENTAL SECTION

Reagents

Iron (II) sulfate-7-hydrate (Sigma Aldrich >99, 5 %, extra pure), ferric chloride hexahydrate (Merck >99%, pro analysis), potassium hydroxide (Merck, pro analysis) and sodium hydroxide (LACHEMA>98%, pro analysis) were used for the synthesis of iron oxide nanoparticles. All chemicals were used as received.

Synthesis

Magnetic iron oxide nanoparticles were synthesized in air, by room temperature co-precipitation of ferrous and ferric salts mixtures in the presence of KOH or NaOH 1 M solution; the reactions were carried out under stirring. In literature are mentioned two types of co-precipitation (I) normal co-precipitation, where alkali solution is dropped into the mixed metal solution (the pH value gradually increase), and (II) reverse co-precipitation, where mixed metal solution is added to alkaline solution (consequently, the pH which is a critical factor in synthesis could be easily controlled at high values) [31]. In order to avoid the pH local altering, reverse co-precipitation was chosen.

Two series of samples, $K_{0.1}$ to $K_{0.0125}$ labeled as the “KOH series”, and $N_{0.1}$ to $N_{0.0125}$ labeled as the “NaOH series” were prepared, the indices refer to the iron concentration. Equi-molar 0.1 M ($K_{0.1}$, $N_{0.1}$), 0.05 M ($K_{0.5}$,$N_{0.5}$), 0.025 M ($K_{0.025}$,$N_{0.025}$) and 0.0125 M ($K_{0.0125}$,$N_{0.0125}$) aqueous solutions of Fe^{2+} and Fe^{3+} were separately prepared, by dissolving ferrous and ferric salts in distilled water (Fe^{2+}/Fe^{3+} ½ molar ratio). Compared to the calculated Fe^{2+}/Fe^{3+} molar ratio, a slight excess of Fe^{2+} was used in the synthesis. The Fe^{3+} solution was first added to the Fe^{2+} solution and stirred (at 400 rpm, for 10 min). Then the solution was rapidly added to the hydroxide solution and stirred for other 30 min. The pH values of the final solutions ranged from 11 to 13. The obtained iron oxide nanoparticles were separated by a permanent magnet, washed with distilled water and, finally, with absolute ethanol. The wet precipitates were dried in air, at 80°C.

Characterization

For particles size and shape determination, TEM investigations were carried out in high contrast operation mode, at 100 kV accelerating voltage, on a High-Tech HT7700 (HITACHI) equipment. The samples were prepared by drop casting diluted nanoparticles dispersed in ethanol, on 300

meshes holey carbon-coated Cu grids (Ted Pella) and vacuum dried. The structure and phase composition of the particles was determined by XRD, using a Ultima IV (RIGAKU) instrument operating with Cu K_α radiation. The crystallite size was calculated using the WPPF method [51] and the instrument influence was subtracted using the diffraction pattern of a Si standard recorded in the same conditions. The Moessbauer spectra were recorded at constant acceleration in transmission mode, with ^{57}Co diffused into an Rh matrix as the moving source. The spectrometer was calibrated to a α-Fe foil standard at 293 K, the isomer shift being expressed with respect to this; the NORMOS program [52] was used to fit the as-recorded spectra. The specific surface area of the powders was measured using the Brunauer-Emmett-Teller (BET) method and the pore size distribution was evaluated from nitrogen desorption isotherms (at 77 K), using the Barrett-Joyner-Halenda (BJH) method; a Nova 1200e (QUANTACHROME) device was used. The magnetic properties were investigated in ac (50Hz) fields of 3.5 kOe amplitude by means of a laboratory-manufactured induction hysteresigraph [53]; the specific magnetization vs applied field curves were recorded to a PC by means of a DT-9816A (DATA TRANSLATION) aquisition card (at 16 bit analog-to-digital resolution) and fitted by assuming a superposition of Langevin functions. The saturation magnetization (technical) was estimated from extrapolating to 50kOe the fitted data.

ACKNOWLEDGEMENTS

The authors thank to Romanian Academy for the financial support: *Program 4. Inorganic compounds and hybrids with relevance in nanostructured materials science. Precursors for advanced materials*.

REFERENCES

1. M. Pastor-Belda, L. Marin-Soler, N. Campillo, P. Vinas, M. Hernandez-Cordoba, *Journal of Chromatography A,* **2018**, *1564*, 102
2. K.D. Kim, S.S. Kim, Y-H. Choa, H.T. Kim, *Journal of Industrial and Engineering Chemistry,* **2007**, *13*, 1137
3. S. Yu, V. M. Hong Ng, F. Wang, Z. Xiao, C. Li, L. Bing Kong, W. Que, K. Zhou, *Journal of Materials Chemistry A,* **2018**, *6*, 9332
4. M. Fiore, G. Longoni, S. Santangelo, F. Panto, S. Sara, P. Frontera, P. Antonucci, R. Ruffo, *Electrochimica Acta,* **2018**, 269
5. R. Gonzales-Rodriguez, P. Granitzer, K. Rumpf, J. L. Coffer, *Royal Society Open Science,* **2018**, *5*, 180697

6. S. Hu, Y. Zhou, Y. Zhao, Y. Xu, F. Zhang, N. Gu, J. Ma, M.S. Reynolds, Y. Xia, H. H. K. Xu, *Journal of Tissue Engineering and Regenerative Medicine,* **2018**, *12*, e2085
7. N. V. S. Vallabani, S. Singh, *3 Biotech,* **2018**, *8*, 279
8. S.P. Schwaminger, S.A. Blanck-Schim, I. Scheifele, V. Pipich, P. Fraga-Garcia, S. Berensmeier, *Biotechnology Journal,* **2018**, e:1800055
9. A.K. Gupta, M. Gupta, *Biomaterial*s, **2005**, *26,* 3995
10. K. El-Boubbou, *Nanomedicine,* **2018**, *13*, 929
11. S. Laurent, D. Forge, M. Port, A. Roch, C. Robic, L. Vander Elst, R.N. Muller, *Chemical Reviews,* **2008**, *108*, 2064
12. R. Massart, *IEEE Transaction on Magnetics,* **1981**, *17*, 1247
13. C. Okoli, M. Sanchez-Dominguez, M. Boutonnet, S. Jaras, M.C. Civera, C. Solans, G.K. Rajarao, *Langmuir,* **2012**, *28*, 8479
14. S. Belaid, D. Stanicki, L. Vander Elst, R.N. Muller, S. Laurent, *Nanotechnology,* **2018**, *29*, 165603
15. J. Ladol, H. Khajuria, H. N. Sheikh, Y. Khajuria, Journal of Chemical Science, **2016**, *128,* 1149
16. R. Dolores, S. Raquel, G-L. Adianez, *Ultrasonics Sonochemistry,* **2015**, *23*, 391
17. N. Tresilwised, P. Pithayanukul, C. Plank, *Journal of Pharmaceutical Science*, **2005**, *32*, 71
18. J. Lodhia, G. Mandarano, N.J. Ferris, P. Eu, S.F. Cowell, *Biomedical Imaging and Intervention Journal*, **2010**, *6***,** e12
19. W. Ramadan, M. Karim, B. Hannoyer, S. Saha, *Advanced Materials Research,* **2012**, *324,* 129
20. N.M. Gribanov, E.E. Bibik, O.V. Buzunov, V.N. Naumov, J*ournal of Magnetism and Magnetic Materials,* **1990**, *85,* 7
21. J.P. Jolivet, L. Vayssieres, C. Chaneac, E. Tronc, *MRS Online Proceedings Library (OPL)*, **1996**, *432,* 145
22. I.M. Bolbokh, G.S. Gunko, G. Yu Yurkov, G.P. Prokhodko, V.A. Tertykh, *Proceedings of the International Conference Nanomaterials: Applications and Properties,* **2013**, *2,* 1
23. S. Alibeigi, M.R. Vaezi, *Chemical Engineering&Technol*ogy, **2008**, *31,* 1591
24. O. Kraagac, H. Kockar, S. Beyaz, T. Tanrisever, *IEEE Transactions on Magnetics,* **2010**, *46,* 3978
25. M. Stoia, A. Tamas, G. Rusu, J. Morosanu, *Studia UBB Chemia LXI*, **2016**, *4*, 147
26. V.K. LaMer, R.H. Dinegar, *Journal of the American Chemical Soc*iety, 1950, **72,** 4847
27. M.C. Mascolo, Y. Pei, T.A. Ring, *Materials,* **2013**, *6*, 5549
28. M. Krizek, J. Pechousek, J. Tucek, K. Safarova, I. Medrik, L. Machala, *AIP Conference Proceedings*, **2012**, *1489***,** 88
29. P.N. Dave, L.V. Chopda, *Journal of Nanotechnology,* **2014**, *398569*, 1
30. Y.Y. Zheng, X.B. Wang, L. Shang, C.R. Li, C. Cui, W.J. Dong, W.H. Tang, B.Y. Chen, *Materials Charact*erization, **2010**, *61*, 489
31. J. Markhulia, S. Kekutia, Z. Jabua, V. Mikhelashvili, L. Saneblidze, SGEM2017 Conference Proceedings, **2017**, *17*, 51

32. M. Manzano, V. Aina, C.O. Arean, F. Balas, V. Cauda, M. Colilla, M.R. Delgado, M. Vallet-Regi, *Chemical Engineering Journal*, **2008**, *137*, 30
33. S. Alibeigi, M. R. Vaezi, *Chemical Engineering&Technology*, **2008**, *31*, 1591
34. E. Murad, J.Cashion, "*Mossbauer spectroscopy of environmental materials and their industrial utilization"*, Springer, Boston, MA, **2004**, chapter Iron oxides.
35. R.E. Vandenberghe, C.A. Barrero, G.M. da Costa, E. Van San, E. De Grave, *Hyperfine Interactions*, **2000,** *126*, 247
36. I. Nedkov, T. Merodiiska, L. Slavov, R.E. Vandenberghe, Y. Kusano, J. Takada, *Journal of Magnetism and Magnetic Materials,* **2006**, *300,* 358
37. F. Rubio, J. Rubio, J.L. Oteo, *Journal of Sol-Gel Science and Technology,* **1997**, *8,* 159
38. I.M.K. Ismail, P. Pfeifer, *Langmuir*, **1994**, *10,* 1532
39. S. Brunauer, L.S. Deming, W.E. Deming, E. Teller, *Journal of the American Chemical Soc*iety, **1940**, *62,* 1723
40. G. Mason, *Proceedings of the Royal Society A Mathematical, Physical and Engineering Sciences,* **1983**, *390,* 47
41. N.E. Velikova, Y.E. Vueva, Y.Y. Yvanova, I.M. Salvado, M.H. Fernandes, *International Scientific Publications: Materials, Methods Technologies,* **2014**, *8*, 162
42. K.S.W. Sing, D.H. Everett, R.A.W. Haul, L. Moscou, R.A. Pierotti, J. Rouquérol, T. Siemieniewska, *Pure and Applied Chemistry,* **1985**, *57*, 603
43. M. Thommes, K. Kaneko, A. V. Neimark, J. P. Olivier, F. Rodroguez-Reinoso, J. Rouquerol, K. S. W. Sing, Pure and Applied Chemistry, **2015**, *87*, 1051
44. K. Praveena, S. Katlakunta, H.S. Virk, *Solid State Phenomena*, **2015**, *232*, 45
45. B.P. Rao, O. Caltun, W.S. Cho, C.-O. Kim, C. Kim, *Journal of Magnetism and Magnetic Materials,* **2007**, *310,* e812
46. H.M.H. El Ghandoor, H.M. Zidan, K. Mostafa, M.I.M. Ismail, *International Journal of Electrochemical Science,* **2012**, *7*, 5734
47. K. Maaz, S. Karim, A. Mumtaz, S.K. Hasanain, J. Liu, J.L. Duan, *Journal of Magnetism and Magnetic Materials,* **2009**, 321, 1838
48. B. Wang, Q. Wei, S. Qu, *International Journal of Electrochemical Science*, **2013**, *8,* 3786
49. G.F. Goya, T.S. Berquó, F.C. Fonseca, M.P. Morales, *Journal of Applied Phys*ics, **2003**, *94,* 3520
50. M. Mandal, S. Kundu, S.K. Ghosh, S. Panigrahi, T.K. Sau, S.M. Yusuf, T. Pal, *Journal of Colloid Interferface Science,* **2005**, *286,* 187
51. H. Toraya, *Journal of Applied Crystallography,* **1986***, 19,* 440
52. R.A. Brand, *Nuclear Instruments and Methods in Physics Research Section B*, **1987**, *28*, 398
53. I. Mihalca, A. Ercuta, *Journal of Optoelectronics and Advanced Materials,* **2003**, *5,* 245